Physics – Uspekhi **53** (8) 789 – 803 (2010)

REVIEWS OF TOPICAL PROBLEMS PACS numbers: 72.15.Jf, 72.20.Pa, 73.50.Lw, 85.80.Fi

Current trends in the physics of thermoelectric materials

A V Dmitriev, I P Zvyagin

DOI: 10.3367/UFNe.0180.201008b.0821

Contents

Abstract. Basic physical ideas and methods that are used to improve the quality of modern thermoelectric materials and to increase the thermoelectric figure-of-merit are reviewed, with special emphasis on how nanostructure affects the thermoelectric properties of materials.

1. Introduction

Energy production and conversion are among the most important activities (and, indeed, the cornerstone of the existence) of human civilization. The primary concern and the subject of continual research and development effort is, of course, to effectively produce electric energy, which is a universal energy form and one the most convenient for practical applications. As the lack of fossil fuel is being increasingly recognized and huge greenhouse gas emissions from organic fuel power plants are producing global climate changes, the efficient conversion of heat energy to electric energy is becoming a problem of vital importance.

In this connection, much attention has been focused on solid-state thermoelectric converters. They offer a number of advantages over traditional electric generators, including design simplicity, the absence of moving parts, low-noise performance, high reliability, and miniaturization with no loss in efficiency. As bidirectional energy converters, they are also used in eco-friendly cooling systems. Currently, however, thermoelectric devices are lower in conversion efficiency compared to the traditional designs of electric generators or refrigerators and have not therefore found wide application in industry. But there exist application areas where the advantages of these devices prevail over the disadvantages. Examples include power sources for spacecraft, wrist watches, portable household refrigerators, electronic, medical, and research equipment (in particular, for cooling infrared detectors and optoelectronic devices), and even seat conditioning devices in high-end cars. However, thermoelectric converters need a considerable increase in efficiency to reach wide industrial application.

The efficiency of a thermoelectric converter is determined by the quantity

$$Z = \frac{\sigma S^2}{\varkappa} ,$$

which has the dimension of inverse temperature and depends only on the physical properties of the converter material [1]. It is sometimes called the 'thermoelectric figure-of-merit,' although this name is more often given to the dimensionless combination

$$ZT = \frac{\sigma S^2 T}{\varkappa} .$$

In the above formulas, σ, S, and $\varkappa$ are respectively the material electrical conductivity, thermopower (Seebeck coefficient), and thermal conductivity, and T is the operating temperature or the average temperature $(T_1 + T_2)/2$ of the converter, with T_1 and T_2 being the respective cold and hot end temperatures. The Ioffe formula reflects the fact that for a given temperature difference, the efficiency of producing electricity becomes higher as the thermopower increases and the nonproductive (i.e., Ohmic and thermal conductivity) losses decrease in the converter. Minimizing these losses

A V Dmitriev, I P Zvyagin Faculty of Physics,
Lomonosov Moscow State University,
Vorob'evy gory, 119991 Moscow, Russian Federation
Tel. (7-495) 939 31 60
Fax (7-495) 932 88 76
E-mail: dmitriev@lt.phys.msu.su, zvyagin@phys.msu.ru

Received 12 November 2009
Uspekhi Fizicheskikh Nauk **180** (8) 821 – 838 (2010)
DOI: 10.3367/UFNr.0180.201008b.0821
Translated by E G Strel'chenko; edited by A M Semikhatov

requires materials with high electric and low thermal conductivity.

Because the thermoelectric figure-of-merit is directly related to the efficiency of a device [1], it is a convenient parameter for comparing the efficiency of converters made of different materials. The value $ZT = 1$ is currently considered to be good at room temperature; passing to 2–3 would mean an increase in efficiency to about 20% and a much larger application range for thermoelectric converters, and thermoelectric devices with ZT equal to 3–4 could likely be competitive in efficiency with electric generators and refrigerating assemblies of conventional design [1].

The currently achieved level of conversion efficiency is determined by the parameters of the best materials used for the purpose.[1] Because no fundamental physical limitations on the efficiency of thermoelectric conversion are known, the search for advanced performance materials is currently in the focus of much attention. The question is how to improve the conversion efficiency.

From the formulas above, a high-quality thermoelectric material must have a high electric conductivity, a high thermopower, and a low thermal conductivity. Because the first two are determined only by the electronic properties of the material, they are often combined into the quantity $P = \sigma S^2$, referred to as the 'power factor.' The thermal conductivity $\varkappa = \varkappa_e + \varkappa_L$, in contrast, is the sum of the electronic ($\varkappa_e$) and lattice ($\varkappa_L$) contributions. It then follows that the thermoelectric figure-of-merit can be maximized by maximizing the electric conductivity and minimizing the thermal conductivity. However, there is a relation between the two, the Wiedemann–Franz law

$$\frac{\varkappa_e}{\sigma} = L_0 T,$$

where L_0 is the Lorentz constant, which has the respective values

$$L_0 = \frac{\pi^2}{3}\left(\frac{k_B}{e}\right)^2 = 2.44 \times 10^{-8}\ \frac{V^2}{K^2},$$

and

$$L_0 = 2\left(\frac{k_B}{e}\right)^2 = 1.48 \times 10^{-8}\ \frac{V^2}{K^2},$$

for electrons obeying degenerate and nondegenerate statistics (k_B is the Boltzmann constant and e is the electron charge). Increasing the electric conductivity not only produces an increase in the electronic thermal conductivity but also usually decreases the thermopower, and hence optimizing ZT turns out to be a challenge. Whereas the power factor can in some cases be increased by varying the concentration of charge carriers in the material, decreasing $\varkappa$ and $\varkappa_L$ is much more problematic, especially for $\varkappa_L$, which is determined by the structure, rigidity, atomic masses, and other characteristics of the lattice.

Metals are highly conductive electrically but have a high thermal conductivity and a low thermopower. Semiconductors and insulators, on the other hand, feature a high thermopower and a small electronic contribution to the thermal conductivity, but both their charge carrier densities and their electrical conductivities are low, leading to a low thermoelectric power factor. Of all the known thermoelectric materials, strongly doped semiconductors or semimetals with the electron concentration about 10^{19} cm^{-3} prove to be the best.

Over the last half century, there has not been much improvement in the thermoelectric characteristics of homogeneous energy conversion materials. The semiconductor alloys $(Bi_{1-x}Sb_x)_2(Se_{1-y}Te_y)_3$, which are among the best industry-produced thermoelectric materials and are widely used in refrigeration devices, still have the room-temperature figure-of-merit around unity, the same as several decades ago. Figures 1 and 2 show the typical thermoelectric figures-of-merit in various temperature ranges for a large number of materials that already are, or potentially can be, used in industry. It is seen that for all the materials, the thermoelectric figure-of-merit lies in the range $ZT < 2$, even at increased temperatures.

For laboratory samples, however, the best achieved values of ZT at room temperature lie in the range 2–3 [3]. The discussion below describes the ways along which this increase has been achieved and the relevant physical ideas. Currently,

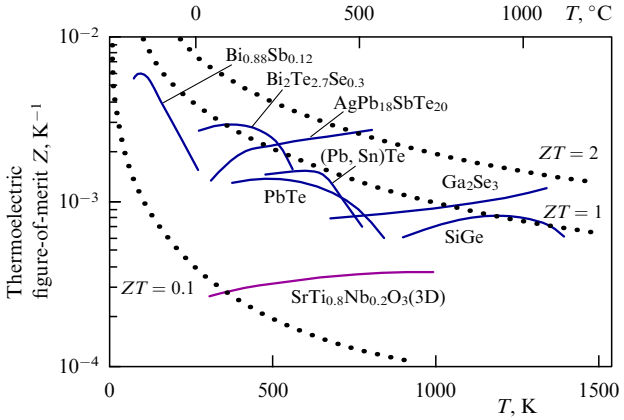

Figure 1. Thermoelectric figure-of-merit of a number of materials currently in use or projected [3].

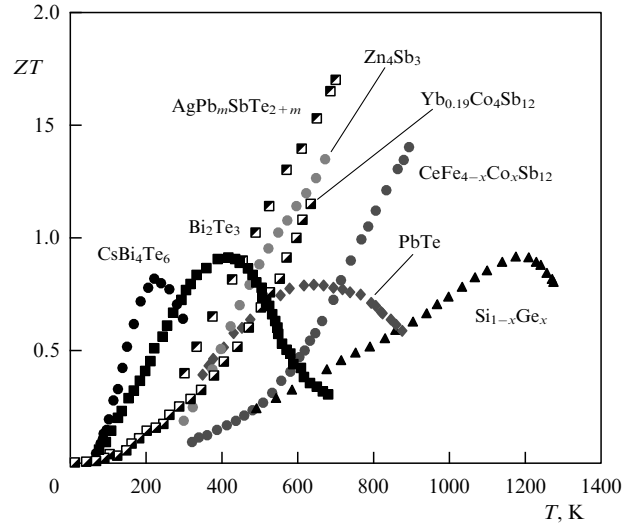

Figure 2. Dimensionless thermoelectric figure-of-merit of a number of widespread or prospective materials [4].

[1] Clearly, the special-purpose design of thermoelectric converters requires solving purely technical design optimization problems. This is not the subject of this review, however. The reader wishing to learn about the design of present-day thermoelectric converters is referred, for example, to Ref. [2].

the best way to improve thermoelectric properties seems to involve spatially inhomogeneous materials with the inhomogeneity size comparable to the characteristic electron or phonon wavelength (which means the nanometer scale).

2. Ways of improving the thermoelectric figure-of-merit of homogeneous materials

In this section, we consider basic physical ideas that have been proposed to increase the thermoelectric figure-of-merit of spatially homogeneous thermoelectric materials, which also include doped materials, solid solutions, and alloys.

2.1 Optimizing carrier concentration

One of the technologically simplest (and therefore virtually universally used) methods of improving the thermoelectric properties of a semiconductor material is to choose the optimum level of doping, where 'optimum' is used in the sense of maximizing the thermoelectric figure-of-merit. As mentioned above, the optimum electron concentration exists because, as the concentration increases, the conductivity usually increases and the thermopower decreases. This decrease can be understood by recalling what mechanisms produce the thermopower.

In the case of a temperature drop across a sample with electronic conductivity, the more energetic and faster hot-end electrons diffuse to the cold end faster than their less energetic and slower cold-end counterparts diffuse in the opposite direction. This gives rise to a flow of electrons from the hot to the cold end, resulting in a negative charge at the cold end and an uncompensated positive charge at the hot end. This is how the bulk thermopower arises.

Clearly, if there are charge carriers of opposite sign in the material, then their contributions to the thermopower weaken one another because both electrons and holes move from the hot to the cold end, but bring charges of opposite sign with them. Therefore, thermoelectric applications require that the material have monopolar conductivity.[2]

We now return to the question of how the thermopower depends on the charge carrier concentration. With increasing the concentration, the gas of charge carriers (e.g., electrons) becomes degenerate when the Fermi level E_F (the electrochemical potential) occurs in the conduction band, and the Fermi energy, i.e., the separation between the Fermi level and the conduction band bottom, exceeds $k_B T$. The energy and velocity of the particles are then determined by the Fermi level position and are almost independent of the temperature, and the flows of the 'hot' and 'cold' electrons therefore differ insignificantly, thus making the thermopower small.

The same conclusion can be reached by another line of reasoning. When the electron distribution becomes degenerate, states deep below the Fermi level are not important, and the electron transport predominantly occurs via states in the energy layer near the Fermi level with the thickness of the order of $k_B T$. Thermopower is related to the Peltier energy Π (energy transfer per electron) by the Kelvin relation $S = \Pi/k_B T$ (see, e.g., Ref. [5]). The Peltier energy is obtained by summing the contributions $E - E_F$ from electron energy levels near the Fermi level; we note that the contribution from the electron states with $E < E_F$ and from the hole states with $E > E_F$ are opposite in sign and can differ in magnitude due to changes in the density of states and in the relaxation time.

[2] Practical applications use both electron- and hole-conducting materials.

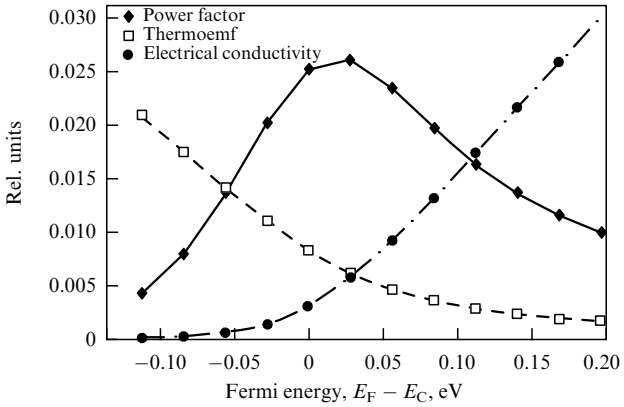

Figure 3. Thermopower, electric conductivity, and power factor as functions of the Fermi energy for PbTe [6].

In the highly degenerate case (for example, in metals), the density of states changes relatively little — and the closer to the Fermi level, the more so; accordingly, the thermopower is small and decreases with increasing the concentration.

Much higher thermopower and thermoelectric figures-of-merit can be expected for semiconductors and semimetals under conditions where the concentration is not too low but the degeneracy is not strong. Figure 3 shows kinetic theory results (including both electron and hole contributions) for the conductivity, thermopower, and figure-of-merit of PbTe, one of the most widespread thermoelectric materials [6]. It is seen that n-PbTe has the maximum figure-of-merit when the Fermi level lies close to the conduction band edge. Here, the degeneracy is not yet strong, whereas the $E > E_F$ and $E < E_F$ charge carriers are highly asymmetric in terms of their densities of states and contributions. We also note that holes, which act to decrease the thermopower in materials with electronic conductivity, turn out to have a low concentration at this position of the Fermi level.

We also note that when conduction is by hopping between localized states, the characteristic hopping energy can be much greater than $k_B T$, such that the thermopower may considerably exceed values found for metallic band conduction [7]. At the same time, the conductivity and the power factor turn out be very small, and therefore thermoelectric converters usually operate in the regime where electron transport occurs by the band mechanism. We consider this mechanism in what follows.

2.2 Optimizing the band gap width

Many semiconductor materials used in thermoelectric converters are alloys or solid solutions whose band structure changes with composition. It then follows that their thermoelectric properties can be optimized by varying the composition and hence the band structure parameters.

One of the major characteristics of the electronic spectrum of a semiconductor is the band gap E_g, and the question of how best to choose its value has repeatedly attracted the attention of researchers. Assumptions on the carrier effective mass dependence on E_g vary from paper to paper, but have proved to have little effect on the results.

If the spectrum is parabolic, there is no relation between these two quantities, and the effective mass is constant. This simple assumption, which works fairly well for semiconductors with an indirect gap in the p space, was made in the

theoretical study in Ref. [8]. It was found that in the case of statistically nondegenerate charge carriers, the best thermoelectric characteristics are obtained for semiconductors with the band gap much larger than $k_B T$. The reason is simple: with this band gap width and with the Fermi level near the conduction band bottom, the concentration of the minority carriers and their contribution to the transport become negligible, thus facilitating an increase in the thermopower as discussed above.

A direct gap, Kane band-structure semiconductor was considered in Ref. [9]. The solution of the electron Boltzmann equation showed that the optimum band gap width (i.e., that maximizing the thermoelectric figure-of-merit) considerably exceeds $k_B T$ and that the optimum Fermi level is near the conduction band edge. The estimate $E_g > 10k_B T$ obtained in the study comes from the fact that narrowing the gap produces holes in the system and thereby decreases the thermopower of the material. The violation of this inequality implies that to prevent the appearance of holes, the optimum Fermi level is to move upwards and into the conduction band; however, this makes the figure-of-merit smaller than in the case of a wider gap (Figs 4 and 5). These conclusions agree quite well with the earlier findings in Ref. [8] for a parabolic band spectrum.

The slight disagreement between Figs 3 and 5 in the position of the optimum Fermi level may be explained by the facts that, first, $E_g < 10k_B T$ in PbTe at room temperature and, second, optimization in Ref. [9] was made with respect to not the power factor P but the thermoelectric figure-of-merit ZT, into which a certain constant value of the lattice heat conductivity was substituted; when the electronic heat conductivity was necessarily decreased, the optimum position of the chemical potential might have moved somewhat down compared with the results in Ref. [6], where only the maximum of the power factor was determined.

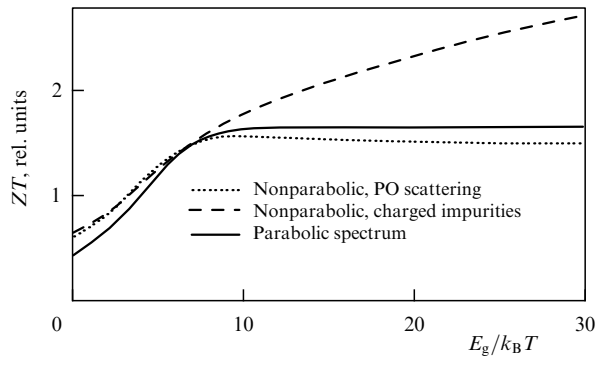

Figure 4. Thermoelectric figure-of-merit as a function of the band gap width for a parabolic and a nonparabilic band model and two electron scattering mechanisms [9].

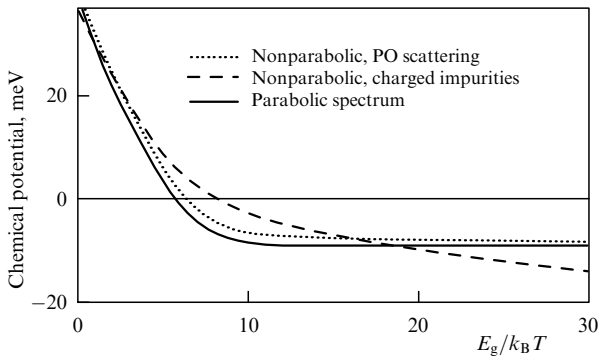

Figure 5. Optimum position of the Fermi level as a function of the band gap width for a parabolic and a nonparabolic spectrum and for two electron scattering mechanisms [9].

The studies mentioned above indicate that in a good thermoelectric material, the spectrum gap must be much greater than the temperature (for example, $E_g > 10k_B T$ [9]) and the Fermi level should lie near the bottom of the majority-carrier band.

In practice, the operating temperatures of thermoelectric devices are somewhat in excess of one tenth of the band gap width. For example, bismuth telluride ($E_g = 0.16$ eV) has its maximum figure-of-merit at 400 K (see Figs 1, 2), and PbTe at 600 K (see Fig. 2), at which its E_g is 0. 36 eV [10].

2.3 Modifying the chemical composition

Another standard way to improve the thermoelectric properties of a material is to modify its chemical composition by preparing its solid solutions or alloys or, alternatively, by growing new chemical compounds on its basis. Notably, this leads to more changes than just a change in the band gap width.

As noted above, PbTe is one of the best materials for thermoelectric generators used in the temperature range 400–800 K [11]. Its alloys with SnTe and PbSe (i.e., the ternary or quaternary systems $Pb_{1-x}Sn_xTe_{1-y}Se_y$) and similar $(GeTe)_{1-x}(AgSbTe_2)_x$ alloys, commonly referred to as TAGS (for the initial letters in the names of the component metals), have for years been the best thermoelectric materials available for operating at about 700 K. From the standpoint of thermoelectric applications, one major advantage of solid solutions over pure materials is a lower lattice thermal conductivity due to the disorder scattering of phonons. For electrons, this disorder is a much weaker factor because, due to their large velocities, their wavelengths are much larger than those of phonons [12].

In contrast, doping PbTe with Group-III elements In, Ga, and Te primarily affects its electronic properties, giving rise to resonance states on the background of the allowed bands [13–15]. From the standpoint of improving the thermoelectric properties, the most interesting situation occurs for Tl doping with the concentration up to 2.0 at. %, when, on the background of the PbTe valence band, an impurity band about 30 meV in width develops about 60 meV below the valence band edge [14] (Fig. 6a). The dramatic changes in the density of states near the impurity band can lead to a significant increase in the thermopower compared to a material without such a band if the Fermi level is positioned appropriately. This can be seen, for example, from the well-known Mott formula [16]

$$S = \frac{\pi^2 T}{3e} \frac{\partial \ln \sigma}{\partial E}\bigg|_{E=E_F} = \frac{\pi^2 T}{3e} \frac{\partial \ln(v^2 g \tau)}{\partial E}\bigg|_{E=E_F}, \qquad (1)$$

valid for degenerate electrons. Here, v, τ, and g are the velocity, the relaxation time, and the density of states of the carriers.

Experiments with $Tl_xPb_{1-x}Te$ samples [17] indeed revealed an increase by a factor of two in the thermoelectric figure-of-merit of $Tl_{0.02}Pb_{0.98}Te$ compared to the original PbTe (Fig. 6b). The thermopower was not observed to increase with increasing the hole concentration in the range $(2.5-5.5)\times10^{19}$ cm^{-3}, nor, importantly, to decrease, con-

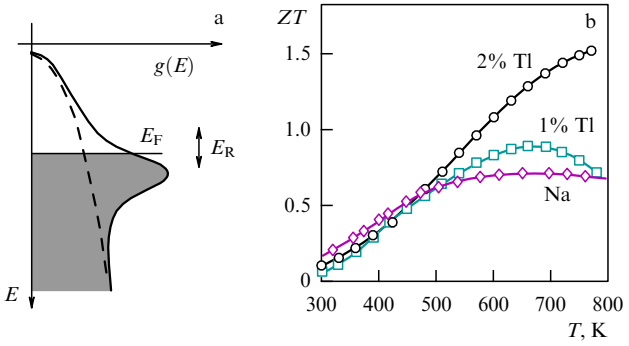

Figure 6. (a) Schematic of the valence-band electronic density of states for PbTe (dashed line) and $Tl_xPb_{1-x}Te$ (solid line); in the latter, the density of states is increased due to Tl levels. The thermoelectric figure-of-merit increases when the hole Fermi level E_F lies in the energy interval E_R near these levels. (b) The measured temperature dependence of ZT in $Tl_{0.02}Pb_{0.98}Te$ and $Tl_{0.01}Pb_{0.99}Te$ compared to that in standard PbTe : Na [17].

trary to what usually occurs for increasing concentration (see Fig. 3). This unusual lack of decrease in S was attributed in Ref. [17] to precisely the increase in the density of states near the Tl impurity band. Whereas the thermal conductivity of $Tl_{0.02}Pb_{0.98}Te$ is independent of the level of doping, the electric conductivity increased with increasing the hole concentration, leading, in the absence of a decrease in the thermopower, to a higher thermoelectric figure-of-merit. [3]

The properties of the original material undergo more profound changes in the alloys of PbTe and $AgSbTe_2$, referred to as LAST. In these alloys, Ag and Sb atoms substitute for Pb to form $AgPb_mSbTe_{2+m}$, a family of semiconductor compounds that show great promise for thermoelectric applications such as the utilization of car engine exhaust heat and the production of electricity from combustible organic fuels. For $m = 10$ or 18 and for the doping level at its optimum value, it was shown in Ref. [19] that such n-type semiconductors have the thermoelectric figure-of-merit $ZT = 2.2$ at 800 K. In that study, the excellent thermoelectric properties of $AgPb_mSbTe_{2+m}$ were attributed to its specific microstructure: according to electron microscopy, it contains regions enriched with 3–5 nm AgSb nanoparticles and shows composition modulations with the period 20–30 nm. Both factors prove to be greatly beneficial to thermoelectric applications, primarily because inhomogeneities enhance phonon scattering and reduce lattice thermal conductivity. The thermal conductivity of these compounds at temperatures above 700 K is less than 1.1 W (m K)$^{-1}$, whereas in PbTe at 300 K, the lattice thermal conductivity alone is 2.3 W (m K)$^{-1}$ [20]. According to a detailed analysis in Ref. [10], just the low thermal conductivity of these alloys is the main reason why their thermoelectric figure-of-merit is about twice that of PbTe. Also, the electronic parameters of the alloy change, and significantly: the conductivity at 800 K decreases about sixfold, and the thermopower increases by a factor of nearly 2.5 compared to PbTe; however, the resulting increase in the power factor at this temperature is only to 28 μW (m K^2)$^{-1}$, to be compared to 25 μW (m K^2)$^{-1}$ in PbTe [10].

Calculations of the electronic band spectrum of $AgPb_mSbTe_{2+m}$ in Ref. [21] show that along with a structural change, the material exhibits a considerable modification in the electron density of states. It turned out that near the valence band top and the conduction band bottom, the density of states profile of $AgPb_mSbTe_{2+m}$ is sensitive to the local ordering of Ag–Sb pairs. Because of the presence of these pairs and due to the appearance of pronounced resonance states, the density of states at the edges of the allowed bands increases faster than in homogeneous PbTe. Therefore, electronic states near the valence band top and the conduction band bottom are of a significantly different nature in $AgPb_mSbTe_{2+m}$ and PbTe. These results, together with electron diffraction experiments [19], indicate that $AgPb_mSbTe_{2+m}$ are not classical solid solutions but unique, heterogeneous, nanostructured systems with a high potential for thermoelectric applications.

A number of complex systems have also been developed based on bismuth telluride Bi_2Te_3; for example, the quaternary compounds $(Bi_{1-x}Sb_x)_2(Se_{1-y}Te_y)_3$ are currently among the most widely used thermoelectric refrigeration materials. Another example is $CsBi_4Te_6$, which grows into needle-shaped crystals and, when doped to the appropriate level, shows a high figure-of-merit, with its maximum value $ZT = 0.8$ at 225 K, which is much below room temperature [22]. This material has the p-type conductivity, the hole concentration of the order of 10^{19} cm^{-3}, and the mobility about 1×10^3 cm^2 (V s)$^{-1}$. The heat conductivity in the needle axial direction is about 1.5 W (m K)$^{-1}$ at 250 K, but the power factor is large, $P = 50$ μW (cm K^2)$^{-1}$, leading to a high figure-of-merit. Band structure calculations for $CsBi_4Te_6$ revealed an indirect band gap equal to 0.08 eV [23]. In Ref. [22], E_g is estimated to be in the range 0.05–0.11 eV. The thermoelectric characteristics of n-type materials are somewhat inferior to those of p-conducting samples. Therefore, the thermoelectric characteristics of $CsBi_4Te_6$ prove to be comparable to those of the bismuth arsenic alloy, one of the best thermoelectric materials for low-temperature applications (see Figs 1 and 2)

The conductivity of most semiconductor compounds and alloys is 1 W (m K)$^{-1}$ = 10 mW (cm K)$^{-1}$ or more [20]. According to the model suggested in Ref. [24], thermal conductivity should be lowest in materials with a low melting point, a large unit cell, and a large average mass of atoms. All these criteria are met in the mixed-valence ternary compound Tl_9BiTe_6, in which Bi^{3+} ions randomly substitute for Tl^{1+} ions in certain lattice sites. The thermal conductivity of this compound is indeed very low, about 0.75 W (m K)$^{-1}$ at 300 K [25]. For the electronic contribution to the thermal conductivity, an estimate using the Wiedemann–Franz law for the measured resistivity 1.6 mΩ cm^{-1} yields $\varkappa_e \approx$ 0.4 W (m K)$^{-1}$ at 300 K, implying that the lattice contribution is 0.3–0.4 W (m K)$^{-1}$.

The authors of Ref. [26] grew Tl_9BiTe_6 samples with the even lower thermal conductivity 0.39 W (m K)$^{-1}$, with the estimated electronic contribution $\varkappa_e$ lower than 0.1 W (m K)$^{-1}$ at room temperature. The hole concentration in this material is $(1.5-2) \times 10^{19}$ cm^{-3}, and the band gap is no less than 0.4 eV. The power factor turned out to be close to 1 mW (m K^2)$^{-1}$ at temperatures 250–400 K, and the thermoelectric figure-of-merit $ZT = 1.2$ at 500 K, to be compared with 0.8 for $Bi_{2-x}Sb_xTe_{3-y}Se_y$ and

[3] We note in this connection that some organic molecules may have sharp peaks in their carrier density of states. If such a molecule is between two metallic electrodes, and if its density-of-state peak is near the Fermi level(s) in the electrodes, then the thermoelectric figure-of-merit is calculated to be extremely high [18].

$(GeTe)_{0.85}(AgSbTe_2)_{0.15}$, which are most widely used at these temperatures.

The significant reduction in thermal conductivity implies the presence of strong phonon scattering in Tl_9BiTe_6. According to the analysis in Ref. [26], this scattering is not due to the small (about 2%) mass difference between bismuth and thallium but due to the difference in their electronic states (Tl^{1+} and Bi^{3+}). Therefore, it can be expected that other materials with randomly distributed atoms of different valences can also have low thermal conductivity.

The search for new classes of good thermoelectric materials is an even more challenging problem than the modification of those already known, and it happens only rarely that a material is promising from this standpoint. Recently, in Ref. [27], a new type of thermoelectric material with many attractive properties was proposed: electron-conducting binary alloys $Mg_2Si_{1-x}Sn_x$, which, similarly to the best current commercial materials, have the high thermoelectric figure-of-merit $ZT = 1.1$ in the temperature range 600–870 K. Compared with commonly used materials, these alloys are advantageous in being low-cost, stable to increased temperatures, technologically feasible, and poison free. Whether they will find wide applications is for the future to tell.

3. Nanostructured materials

A major avenue in which thermoelectric material studies have shown considerable progress in recent years is the use of inhomogeneous materials. Importantly, there are factors that complicate the electron kinetics in such materials, one example being circular currents whose magnitude depends on the structure and geometry of the system [28]. However, introducing the size of a component as an additional parameter of the system simplifies the problem of improving the thermoelectric figure-of-merit.

As noted above, in the presence of inhomogeneities, the lattice thermal conductivity can increase due to phonon scattering on interfaces, and the power factor, determined by electrons and holes and their interaction with phonons and other scatterers, can simultaneously increase (we discuss this is more detail in what follows). Both factors can lead to an increase in the thermoelectric figure-of-merit.

Nanostructured systems are of considerable interest for thermoelectric applications. They include superlattices, quantum-well, quantum-wire, and quantum-dot structures, and a wide variety of composites with irregular nanosized inclusions. Although the first to attract attention were regular structures, which are easier to treat theoretically, lower-cost and easier-to-produce composites have started to seem more promising in recent years.

4. Superlattices and quantum-well systems

4.1 Electronic properties

Calculations in Refs [29–31] for quantum-well and quantum-wire systems showed that the power factor and thermoelectric figure-of-merit are affected by changes in the electron density of states due to dimensional reduction. Later [32–34], quantum wire and dot superlattices also attracted attention. Calculations predicted that reducing wells and wires in transverse size leads to considerably larger P and Z due to a thermopower increase resulting from a density of states feature at the bottom of the lowest confinement subband.

Equation (1) does indeed imply that using features in the density of states in systems of reduced dimensionality (for example, a step near the bottom of the dimensional-quantization band in a two-dimensional system) can lead to a much more asymmetric density of states, thus allowing the thermopower to be increased by moving the Fermi level with respect to these features. Such an increase was discovered experimentally in $PbTe/Pb_{1-x}Eu_xTe$ superlattices in Refs [31, 35]. Just this effect initially caused researchers to pin hopes on lower-dimensional systems.

It was found later, however, that the approximations Hicks and Dresselhaus used in their early calculations ignored some important aspects in the kinetics of charge carriers in real lower-dimensional systems. In particular, Hicks and Dresselhaus assumed that a layer is an infinitely deep potential well for electrons, and used the constant relaxation time approximation when considering electron scattering (which implies that the carrier mobility remains unchanged with decreasing the layer thickness). It turned out that dropping these assumptions can change the calculated thermoelectric parameters considerably.

In Refs [36–38], for example, the Kronig–Penny model was used to consider structures with finite-depth wells while keeping the constant relaxation time approximation for scattering. It was found that for a finite height of barriers between the wells, the power factor first increases with decreasing the well width and then starts to decrease due to electrons tunneling through the barriers, and passes through a maximum at an intermediate thickness. Another finding was that the power factor decreases markedly with decreasing the barrier height.

Calculations in Refs [39, 40] for PbTe took a number of factors into account, such as the lifting of the fourfold degeneracy of the valleys due to confinement, and the strong increase in electron scattering with decreasing the well width, due to both scattering on hetero-interfaces and the increased probability of scattering on deformation acoustic phonons in thin layers. In accordance with the uncertainty relation, the more spatially localized an electron is, the larger the average value of the electron momentum component normal to the layer (this component does not have a definite value). This increases the phase volume of those phonons with which charge carriers can interact, and thus enhances acoustic scattering [41]. Including these factors have shown, for PbTe-based quantum dot systems, that the power factor in narrow wells may even decrease compared to that in homogeneous PbTe [39, 40].

Pshenai-Severin and Ravich [42] showed that in a layer in the presence of confinement, the LA phonon scattering relaxation time τ decreases in the elastic approximation in proportion to the layer thickness L and can become much smaller than in a three-dimensional crystal,

$$\frac{\tau_{2D}}{\tau_{3D}} = \frac{2kL}{3\pi} ,$$

where k is the electron wave number. Similar results were obtained in the case of impurity scattering. Thermoelectric figure-of-merit calculations for multilayer quantum dot systems for elastic electron scattering on acoustic phonons and short-range impurities showed that the increase in kinetic coefficients and the thermoelectric figure-of-merit, due to the density of states changing its shape as a result of confinement,

is fully compensated by the decrease in the relaxation time. Moreover, it turned out that if the chemical potential is in each case chosen from the condition of maximizing the figure-of-merit, then a multilayered structure and a bulk crystal have fully identical expressions for the thermoelectric figure-of-merit. Hence, the idea of Hicks and Dresselhaus turned out to be less general than originally expected and inapplicable to some important cases.

Under some conditions, however, Hicks and Dresselhaus' predictions can remain valid. It was shown in Ref. [43] that if the dominant electron scattering mechanism is the coupling to polar optical phonons, then at high temperatures, when PO scattering can be considered elastic, the corresponding electron relaxation time remains constant with decreasing the well thickness, and Hicks and Dresselhaus are then correct in predicting a large thermoelectric figure-of-merit for quantum-well systems. Physically, the reason for this is that with the PO mechanism, the scattering probability decreases with increasing the momentum transferred to the scatterer (the transferred momentum increases with decreasing the layer thickness).

There are other ways as well to improve the thermoelectric characteristics of quantum-well systems compared to those of bulk samples. An important finding was that DA scattering changes its nature with decreasing the layer thickness [44]. The reason is that an increase in the average electron momentum with decreasing the layer thickness (discussed above in connection with Refs [39–41]) leads not only to an increase in the phase volume of phonons with which charge carriers can interact but also to an increase in the energy of these phonons. As a result, the elastic approximation used in earlier works can be insufficient for describing acoustic scattering in a narrow well. For this reason, the layer conductivity was calculated in Ref. [44] by taking the inelastic scattering of two-dimensional electrons on acoustic phonons into account, with the acoustic phonons considered three-dimensional, as in a homogeneous material.

It turned out that a quantum-well system with the well thickness L and a homogeneous material of the same composition have the conductivity ratio that depends on a single parameter $t = TL/\pi\hbar s_{\parallel}$, where $s_{\parallel}$ is the longitudinal speed of sound. The calculated conductivity ratio is virtually unity for $t > 1$, i.e., for relatively wide wells, and increases when t becomes less than unity. For quantum wells 2 nm in thickness, this second region corresponds to temperatures less than 50 K; hence, the thermoelectric figure-of-merit can be increased by this mechanism only at low temperatures.

4.2 Phonon properties

The discussion was so far limited to the electronic properties of quantum-well systems; however, the nanostructure is reflected not only in the electronic but also in the phonon, or lattice, properties of the sample. Nanosized inhomogeneities are effective scatterers of thermal phonons, which are also in the nanometer wavelength range, and hence act to reduce the thermal conductivity. The effect of nanostructure on the lattice thermal conductivity has been the subject of much study because reducing thermal conductivity is crucial for increasing the thermoelectric figure-of-merit.

That the lattice thermal conductivity of a superlattice may be reduced compared to the homogeneous material was noted in Ref. [45], where the selective transmission of high-frequency phonons across a superlattice was studied. Such a decrease in thermal conductivity was directly observed in transverse thermal conductivity measurements on Si/Ge superlattices and thin films of the $Si_{0.85}Ge_{0.15}$ alloy [46]. The thickness of Si and Ge layers in various superlattice samples was in the respective ranges 13–146 and 5–54 monoatomic layers, and the measurement temperature was varied between 80 and 400 K. Superlattices with the period 30–300 Å had the thermal conductivity around 2 W (m K)$^{-1}$, which is about half the value for $Si_{0.85}Ge_{0.15}$, whose films had the thermal conductivity 4–5 W (m K)$^{-1}$, the same as found in its bulk samples. The thermal conductivity of superlattices with the period 30–65 Å turned out to be 3–4 W (m K)$^{-1}$, much higher than in long-period lattices.

A similar decrease by about a factor of two in the effective thermal conductivity in the direction normal to the layer was observed in Bi_2Te_3/Sb_2Te_3 superlattices with the period 40–120 Å [47]. The dependence of the thermal conductivity on the superlattice period was found to be small and lie within experimental error.

General considerations suggest that for layer thicknesses considerably larger than the phonon mean free path, the thermal conductivity should approach the weighted average of the thermal conductivities of the individual layers. But if the layers are very thin or, in the limit case, monoatomic, then the thermal conductivity should be close to that of an alloy of the corresponding composition. For intermediate thicknesses, comparable to the wavelength of thermal phonons, thermal conductivity may decrease due to the Bragg scattering of phonons at layer interfaces.

The detailed study in Ref. [48] of the lattice period dependence of the lattice thermal conductivity of Bi_2Te_3/Sb_2Te_3 structures in a wide range of periods (20–180 Å) revealed just such a decrease. The lowest value of conductivity in the stacking direction, less than 0.4 W (m K)$^{-1}$, was observed for the lattice period 60 Å. The Wiedemann–Franz result for the lattice part of thermal conductivity turned out to be much less than in homogeneous solid solutions (alloys), its minimum value 0.25 W (m K)$^{-1}$ corresponding to the superlattice period about 50 Å. At smaller periods, the thermal conductivity increased and reached the value 0.4–0.5 W (m K)$^{-1}$, characteristic of $BiSbTe_3$ alloys, at 20 Å. For larger periods, however, the lattice thermal conductivity of the superlattices became markedly larger than in the alloys, approaching a value typical of homogeneous Bi_2Te_3 and Sb_2Te_3 ($\varkappa_L = 1.05$ and 0.96 W (m K)$^{-1}$, respectively).

The observed decrease in the transverse phonon thermal conductivity of superlattices is apparently not the limit. According to theoretical calculations in Ref. [49], superlattices with a complex unit cell and not with just two but with three, four, or more layers in each period [50] are candidates for further decreasing the thermal conductivity.

The possibility of such a large decrease in the transverse thermal conductivity of superlattices naturally generated interest in how this affects their thermoelectric properties. The answer was given in Ref. [51], which reported a record increase in the thermoelectric figure-of-merit for p-conducting Bi_2Te_3/Sb_2Te_3 superlattices to $ZT = 2.4$ at 300 K. The layer thickness in these superlattices was 10 Å for bismuth telluride and 50 Å for antimony telluride. Most of the figure-of-merit increase is precisely due to the significant decrease (to 0.22 W (m K)$^{-1}$) in the lattice thermal conduction. It is important that a superlattice structure, while considerably changing the phonon properties, has practically no effect on the hole mobility, whose value 380 cm^2 (V s)$^{-1}$ is the same both along and across the layers. The superlattice hole

mobility was found to be several times larger than in $BiSbTe_3$ (where it is less than 100 cm^2 $(V\ s)^{-1}$) and is comparable to that in homogeneous Sb_2Te_3 [51, 52].

We note that n-conducting $Bi_2Te_3/Sb_2Te_{2.83}Se_{0.17}$ superlattices studied in the same work showed much poorer performance at the same layer thicknesses. They were found to have a higher lattice thermal conductivity, $\varkappa_L = 0.58$ W $(m\ K)^{-1}$, and a lower electron mobility characteristic of an alloy, with the result that their thermoelectric figure-of-merit was significantly lower, $ZT = 1.4$ at 300 K. The authors of the study suggest that the interfaces in n-type structures that contained the solid solution were of insufficient quality to reflect phonons specularly. Nevertheless, the gain by a factor of almost 1.5 in the figure-of-merit was achieved over the homogeneous samples of the same material, primarily, again, because of the reduced thermal conductivity in the stacking direction.

Because they operate at room temperatures, bismuth-telluride-based devices are mainly used in various refrigerating systems. Materials for use in thermoelectric generators should be able to operate at higher temperatures; one example is lead telluride. The thermoelectric properties of n-conducting $PbTe/PbTe_{0.75}Se_{0.25}$ superlattices with the electron concentration 1×10^{19} cm^{-3} were investigated in Ref. [53]. Experiments on optimized samples with a perfect superlattice structure with the period about 70 Å showed a decrease in the lattice thermal conductivity to 0.5 W $(m\ K)^{-1}$, which is about half the value for films of the $PbTe_{0.75}Se_{0.25}$ alloy, and one third of the value for PbTe films. The electron mobility along layers was about 700 cm^2 $(V\ s)^{-1}$, independent of the superlattice period. This is about the same as that found in the $PbTe_{0.75}Se_{0.25}$ alloy but nearly half the value for PbTe films. Using the measured electronic characteristics of this superlattice, its thermoelectric figure-of-merit was estimated to be $ZT = 0.63$ for 300 K in the stacking direction and $ZT = 1.75$ for 425 K parallel to the layers, whereas for bulk PbTe, the respective values of ZT at these temperatures are 0.40 and 0.70.

We note that the lattice component of the superlattice thermal conductivity is usually obtained by first measuring the total thermal conductivity and then subtracting the electron contribution calculated from the Wiedemann–Franz law. As is known, this law is valid for charge carriers scattered elastically [5]. Because of the strong inelastic scattering by longitudinal optical phonons in lead telluride at room temperature, the results obtained for PbTe using this law should be treated with caution. Besides, it has recently been shown that the Lorentz constant in superlattices can be considerably different from its value in a homogeneous and isotropic material and can even oscillate with changing the layer thickness [54]. The earlier studies cited above did not, of course, take this fact into account when segregating the lattice component of thermal conductivity. This remark does not affect calculations of the thermoelectric figure-of-merit, however, which involves only the total thermal conductivity.

5. Quantum wires

Quantum wires and their arrays are another subject of recent interest for possible thermoelectric applications. Similarly to superlattices, the presence of heterointerfaces changes the electronic and phonon properties of quantum-wire systems.

Quantum wires may have a much higher power factor compared to both bulk materials and quasi-two-dimensional layers. The reason is that charge carriers in quantum wires experience stronger quantum confinement, resulting in the density of states having sharp features near the edge of the allowed band. It is shown theoretically in Ref. [29] that the thermoelectric figure-of-merit of a quantum wire depends strongly on the wire thickness. A considerable increase in the figure-of-merit occurs at thicknesses less than the thermal de Broglie wavelength of the electron. For Bi_2Te_3 wires of the thickness 5 Å, the room temperature figure-of-merit ZT reached a value about 14, compared with 0.7 for bulk samples under the same conditions (as was the case for quantum wells, the constant relaxation time approximation was used in the calculations).

This conclusion was confirmed in a later theoretical study [55], where a simplified band structure model of Bi was developed and modified for the one-dimensional system to calculate how the band structure and thermoelectric properties of bismuth wires vary with the thickness. Specifically, a nanowire of a square cross section, grown along the trigonal axis, was considered. The calculation (still in the constant relaxation time approximation) has shown that by appropriately choosing the wire thickness and electron concentration, a marked increase in the thermoelectric figure-of-merit can be achieved for small thicknesses.

Similar results were obtained in Ref. [32], where a theoretical model of electron transport in quantum bismuth wires of a cylindrical shape was developed. Based on the Bi band structure and again using classical transport theory in the constant relaxation time approximation, the authors of Ref. [32] calculated ZT for wires of various diameters and crystal orientations. The results showed that thermoelectric applications favor trigonal-axis-oriented wires with the diameter less than 10 nm, $ZT > 1$. The investigation of the role of heavy holes in the T extremum demonstrated that ZT might be considerably increased, especially for a p-type material, if their concentration could be decreased.

This last finding naturally suggests using $Bi_{1-x}Sb_x$ alloy nanowires instead of those grown from pure Bi because such an alloy is, in a certain composition range, a direct-gap semiconductor with carriers at the L extrema only. Electron transport for $Bi_{1-x}Sb_x$ $0 < x < 0.30$ alloy wires with the diameter 10–100 nm at 77 K was calculated in [56]. Also calculated was the band diagram for such wires, showing how energy band edges in a wire change their position with changing the wire thickness and the alloy composition. Using the same methods and approximations as in Refs [32, 55], it was found that the thermoelectric figure-of-merit of $Bi_{1-x}Sb_x$ nanowires should be higher than in bismuth wires and bulk bismuth. The highest value, $ZT = 1.2$ at 77 K, was found for p-type wires 35–45 nm in diameter for $x \approx 0.13-0.14$. The explanation given was the coincidence of about ten valence band subbands, resulting in a large density of states near the Fermi energy. Therefore, there was no monotonic increase in ZT with decreasing wire diameter.

We note, however, that some care is needed in analyzing the conclusions obtained in the constant relaxation time approximation in the studies cited above. As already noted in the section on superlattices, quantum-well calculations using the same approximations are valid only when the dominant scattering is by optical phonons [42, 43]. More accurate quantum-wire results were obtained in subsequent studies [57, 58], but we postpone this until a discussion of the phonon properties of wires.

The studies reviewed above in this section primarily focused on the electronic properties of nanowires. It is clear, however, that interfaces in wires, similarly to superlattices, can also enhance phonon scattering, reduce the thermal conductivity, and increase the thermoelectric figure-of-merit.

A significant decrease in the wire thermal conductivity compared to that of the bulk material was predicted theoretically in Ref. [59], where a solution of the Boltzmann equation was used to calculate the lattice thermal conductivity of a free wire. The diffuse and specular phonon scattering from the wire surface were simulated by imposing appropriate boundary conditions on the phonon distribution function. The example considered was a free GaAs wire at room temperature. It was shown that the effect of an increase in thermal conductivity with the thickness is more pronounced in wires than in planar layers. The explanation is that a wire has a higher surface-to-volume ratio than a layer, which produces more phonon surface scattering and decreases the thermal conductivity.

Measurements of the longitudinal thermal conductivity of free Si wires [60] provided experimental support for these conclusions. Although the wires studied were definitely crystalline in structure, their thermal conductivity was found to be much lower (by more than two orders of magnitude) than that of bulk samples. It was observed that decreasing the wire diameter strongly reduced its thermal conductivity and changed its temperature dependence. The explanation suggested was that the phonon mean free path decreases due to surface scattering and, possibly, that phonons in the thinnest wires change their spectrum due to quantum constraints on their motion.

The last possibility is suggested by the following factors. At low temperatures, the temperature dependence of the thermal conductivity of wires 115 and 56 nm in diameter is well described by a cubic law that follows from the kinetic theory formula [61]

$$\varkappa_{\mathrm{L}} = \frac{1}{3}\, c\rho \langle v_{\mathrm{ph}} \rangle\, l_{\mathrm{ph}},$$

where c is the heat capacity of the material, ρ is its density, $\langle v_{\mathrm{ph}} \rangle$ is the mean phonon velocity, and l_{ph} is the phonon mean free path. If l_{ph} is constant and is determined by the wire thickness, then this formula implies that $\varkappa_{\mathrm{L}} \sim c \sim T^3$. But the thermal conductivity of wires 37 and 22 nm in diameter increases with the temperature more slowly, which is hardly explained by boundary scattering alone and likely points to a change in the wire phonon spectrum due to quantum dimensional effects.

Lattice thermal conductivity calculations in Ref. [62] for crystalline Si nanowires similar to those studied in Ref. [60] used the fully realistic phonon spectrum, with no cutoffs of the type introduced in the Debye model, and used only the experimental characteristics of the bulk material, not those obtained for nanowires. The results agree well with the experimental data in Ref. [60] for wire thicknesses more than 35 nm, when the confinement of phonons is of little significance. On the other hand, it turns out that the simpler Callaway formula [63], based on the idea of a dispersionless phonon spectrum, also adequately describes these experimental data if the uppermost phonon frequency is taken to be much less than the Debye frequency in silicon. The reason is that the real spectral density of high-frequency phonons in this material is much lower than that given by the Debye model.

Nanowires of other materials can also be expected to exhibit a considerable decrease in thermal conductivity if their thickness becomes less than the phonon mean free path in the homogeneous material. These expectations were supported by lattice thermal conductivity calculations for III–V and II–VI semiconductor nanowires [64]. Using the method developed in Ref. [62], it was shown that for all ten materials studied (GaAs, InSb, In P, InAs, AlSb, GaSb, CdTe, ZnS, ZnTe, and ZnSe), the thermal conductivity of a 30 nm wire is about an order of magnitude lower than that in the bulk sample. The authors show that the amount of this decrease for a particular binary compound depends on the mass ratio of the component atoms and can be described by the approximate formula

$$\frac{\varkappa_{\mathrm{wire}}}{\varkappa_{\mathrm{bulk}}} \sim \left(1 + \frac{M_{\mathrm{lighter}}}{M_{\mathrm{heavier}}}\right)^{3/2},$$

where $\varkappa_{\mathrm{wire}}$ and $\varkappa_{\mathrm{bulk}}$ are the thermal conductivities of the wire and the homogeneous material, and M_{lighter} and M_{heavier} are the masses of the lighter and the heavier component atoms.

With the availability of data collected on the electronic and phonon properties of nanowires, the study of their thermoelectric characteristics was put on the agenda. The detailed theoretical investigation [57, 58] of the thermoelectric properties of III–V semiconductor nanowires showed that their power factor increases with decreasing the thickness, but only in a limited way, similar to that obtained in Ref. [40] for lower-dimensional PbTe-based systems (see Section 4.1). Based on the Boltzmann kinetic equation and without invoking the constant relaxation time approximation, the thermal and electronic properties of nanowires were calculated. It can be seen from Fig. 7 that the power factor rapidly increases over a certain range of decrease in the wire thickness and then tends to a final limit value. Rapid increase starts when all carriers are concentrated in a single confinement subband, and therefore the wire thickness corresponding to this start is proportional to the inverse value of the electron effective mass in the material. Therefore, the increase in the power factor with decreasing the thickness starts first in InSb, followed by InAs and, finally, by the thinnest GaAs and InP wires. The power factor ceases to grow in the limit of small

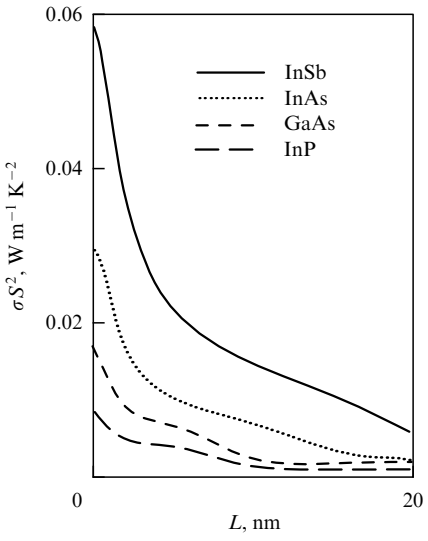

Figure 7. Power factor of a nanowire as a function of its thickness for four optimally doped III–V materials at room temperature [58]. The power factor increase at small thicknesses is evident.

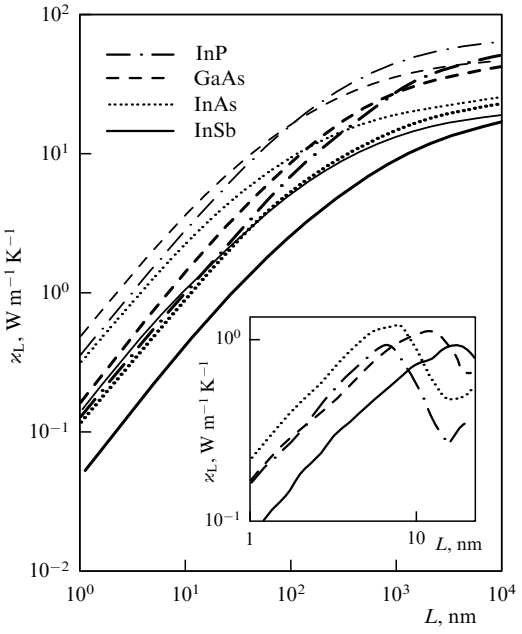

Figure 8. Lattice thermal conductivity as a function of the thickness for InSb, InAs, GaAs, and InP nanowires [58]. Solid (dashed) lines: diffusion (partially specular) scattering of phonons on wire boundaries. The inset shows the electron contribution to the thermal conductivity.

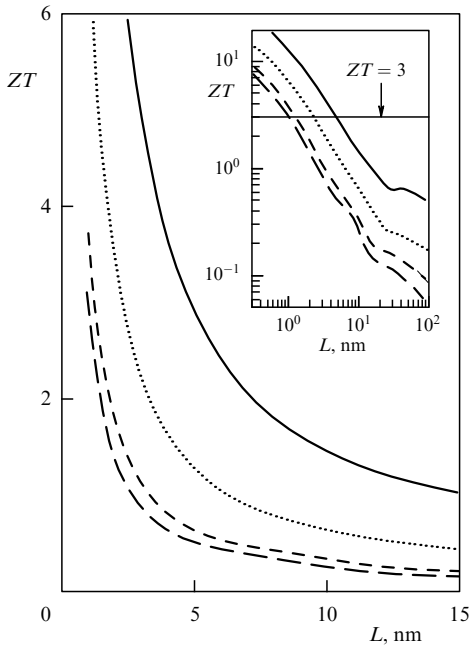

Figure 9. The calculated figure-of-merit ZT as a function of the quantum wire thickness for diffusive phonon scattering on wire boundaries for InSb, InAs, GaAs, and InP wires [58]. Inset: the increase in ZT in a logarithmic scale. The notation is the same as in Fig. 8.

thicknesses because the deformation potential scattering of electrons rapidly grows in intensity with decreasing the wire thickness. For InSb, the calculation of the power factor in the limit of small thicknesses gave 20 times the bulk value.

Figure 8 shows the calculated [58] dependence of the lattice thermal conductivity $\varkappa_L$ on the nanowire thickness for four different materials. Phonon scattering on wire boundaries was considered to be diffuse. As seen from the thin lines, the more specular the scattering is, the higher the thermal conductivity. The calculated thermal conductivity $\varkappa_L$ depends linearly on the thickness as long as the thickness is small, due to the predominance of the boundary phonon scattering; at larger thicknesses, $\varkappa_L$ is equal to the thermal conductivity of the bulk material.

Figure 9 reproduces the plots of ZT as a function of the wire thickness obtained in [57, 58] using the thermal conductivity and electron thermoelectric quantities calculated by solving the Boltzmann equation. It is seen that the only potential candidate for thermoelectric applications is InSb, whose wires, with thicknesses 5–10 nm, can provide a sufficiently high thermoelectric figure-of-merit. The power factor turns out to increase 10–20-fold with decreasing the wire thickness and the remaining part of the calculated figure-of-merit increase is due to the increased thermal conductivity.

A question that arises from the above is whether, in addition to affecting the phonon transport, boundary scattering affects the electron transport in nanowires. At room temperature, the thermal wavelength of electrons is of the order of tens of nanometers, whereas that of phonons is less than 1 nm. Accordingly, a subnanometer rough surface is rough for phonons and virtually smooth for electrons. We note that, as can be seen in Fig. 8, the electron contribution to the thermal conductivity is not small at small wire thicknesses.

Free nanowires are impractical for use, however, and this could be the reason underlying the proposal in [65, 66] that the thermoelectric figure-of-merit could be increased using a composite in which the matrix of a thermoelectric material, InSb or PbTe, contains an ordered array of mutually parallel weakly conducting nanowires that form a rectangular lattice in the matrix. It turned out that due to the dimensional quantum effect for the electrons of the matrix, it is indeed possible to increase the power factor by appropriately choosing the structural parameters, the lattice period, and the wire thickness. Compared with the material of the matrix, the power factors of PbTe- and InSb-based composites were calculated to be 2.5 and 3.5 times larger for the structural period 5–10 nm and room temperature.

So far, experimental studies on the thermoelectric properties of nanowires have been fewer than the theoretical ones. An increase in the thermopower in composites with 9 and 15 nm bismuth nanowires in a porous aluminum oxide or silica gel was first observed experimentally in [67]. Based on the temperature dependence of their electric resistance, these samples were identified as semiconductors with the band gap 0.17–0.4 eV. For samples with 15 nm wires in SiO_2, the thermopower was negative, and at 100 K, its absolute value is about 1×10^4 μV K^{-1}, decreasing to 50 μV K^{-1} at 300 K (the last value is for bulk bismuth). In samples with 9 nm Bi wires in Al_2O_3, the thermopower was positive and in excess of 2×10^4 μV K^{-1} at temperatures 100–300 K; in one of the samples, the value 2×10^5 μV K^{-1} was observed.

The measurements in Ref. [68] were made on Bi_2Te_3 nanotubes in the form of hydrothermally synthesized powder. The presence of an inner channel in a nanotube can additionally complicate the propagation of phonons and decrease their thermal conductivity compared to nanowires. The measured thermoelectric figure-of-merit ZT of compressed Bi_2Te_3 power appeared to be close to unity, i.e., about 20% above that in the best commercial Bi_2Te_3.

There has also been much recent effort to experimentally investigate silicon nanowires, which are the easiest to produce.

The preparation of single-crystalline n- and p-conducting nanowires 20–300 nm in diameter was reported in [69]. The electronic properties of silicon nanowires were found to be almost the same as in the bulk, such that the power factor changed little, but their thermal conductivity turned out to be an order of magnitude less. As a result, the thermoelectric figure-of-merit at room temperature of a 50 nm nanowire increased to 0.6.

As a wire decreases in diameter, its thermoelectric figure-of-merit becomes still higher; for example, for 20 nm nanowires optimized with respect to the level of doping ($p = 3 \times 10^{19}$ cm^{-3}), it proved possible to obtain the value $ZT \approx 1$ at 200 K [70]. A further increase in the figure-of-merit with a decrease in the diameter of a silicon wire was predicted in Ref. [71], specifically to the value $ZT = 3$ at 300 K for 2 nm wires.

6. Nanocomposites

It is clear from the above discussion that one of the most important changes that occur to the physical properties of heterostructures and lower-dimension systems and that can lead to an increase in the thermoelectric figure-of-merit is the reduction in thermal conductivity due to phonon scattering on surfaces and heteroboundaries. But there also exist other ways to decrease the lattice thermal conductivity, unrelated to the costly and complex process of growing a superlattice or a quantum-well or quantum-wire structure. It has already been mentioned that substitutional atoms in alloys effectively scatter phonons, thereby reducing the thermal conductivity of crystalline substances to the so-called alloy limit [72]. The same role can be played even more effectively by nanosized inhomogeneities.

Clearly, a nanocomposite containing such inhomogeneities undergoes changes in both its phonon and its electronic properties, and the latter change also affects the thermoelectric characteristics of the nanocomposite. We first consider the thermal conductivity.

It is already clear from the Rayleigh formula for the scattering cross section $\sigma \sim a^2/\lambda^4$ (where a is the scatterer size and λ is the wavelength) that if point-like defects in the alloy are effective in scattering short-wavelength phonons, then nanoparticles additionally scatter middle- and long-wavelength phonons, possibly resulting in a much reduced thermal conductivity. Additional support for this conclusion came from a more sophisticated theoretical model developed in Ref. [73]. In the same study, $In_{0.53}Ga_{0.47}As$ with ErAs inclusions 1–4 nm in size were measured to have a thermal conductivity nearly two times lower than the alloy limit and a higher thermoelectric figure-of-merit by a factor of two.

It turns out that to decrease the lattice thermal conductivity, it is by no means necessary that the nanoinclusions be arranged in an orderly manner. Figure 10 (reproduced from Ref. [74]) shows the calculated results for the thermal conductivity of Ge/Si structures with inclusions of various sizes and shapes. It can be seen from the figure that the thermal conductivity is virtually independent of both the specific structure of the nanocomposite and the arrangement of the inclusions, and depends only on the area of interfaces per unit volume, determined by the concentration and size of the inclusions. It is also seen that the thermal conductivity of a nanocomposite may be much less than the minimum value for an alloy of the same components, suggesting good prospects

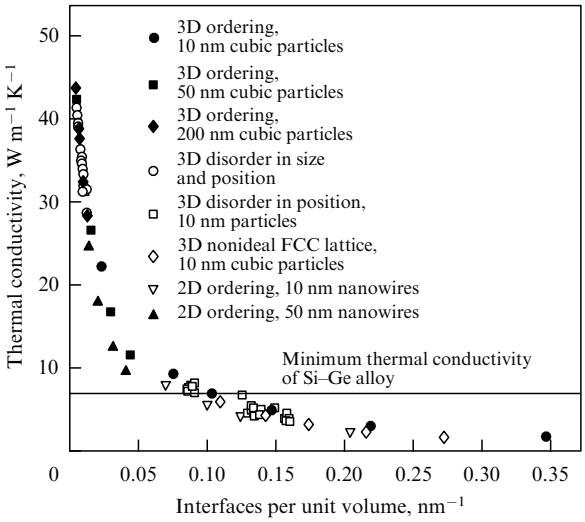

Figure 10. The calculated thermal conductivity of nanostructured materials with inhomogeneities of various sizes and shapes as listed in the inset [74].

for using nanocomposites to increase the thermoelectric figure-of-merit.

Measurements of the thermoelectric properties of $Zr_{0.5}Hf_{0.5}Ni_{0.8}Pd_{0.2}Sn_{0.99}Sb_{0.01}$ nanocomposites with ZrO_2 particles about 20 nm in diameter in the temperature range 300–900 K [75] indeed showed that their thermal conductivity decreased with the content of ZrO_2 particles quite considerably, from 3.6 W (m K)$^{-1}$ in their absence to 2.5 W (m K)$^{-1}$ at the 9% volume content. These values refer to the temperature 700 K, at which the thermal conductivity has a minimum for all nanoparticle concentrations. The decrease in thermal conductivity is to a large extent due to the lattice component and is likely explained by the fact that nanoinclusions effectively scatter thermal phonons, the dominant heat carriers in ZrNiSn-based alloys. The estimate of the lattice thermal component obtained from the Wiedemann–Franz law is $\varkappa_L \approx 0.7$ W (m K)$^{-1}$ at 800–900 K.

A decrease in thermal conductivity and a corresponding increase in the thermoelectric figure-of-merit have also been observed in nanostructured samples of Si and $Si_{0.95}Ge_{0.05}$ with the grain size 10–30 nm. The thermal conductivity of nanostructured Si samples was found to be an order of magnitude higher than that in bulk crystalline silicon, and introducing 5% of Ge atoms produced an additional increase in the scattering of short-wavelength phonons and led to a further twofold decrease (to 5–6 W (m K)$^{-1}$) in thermal conductivity. As a result, nanostructured $Si_{0.95}Ge_{0.05}$ reached the thermoelectric figure-of-merit 0.95 at 900 K [76].

But the reduced lattice thermal conductivity is not the only consequence of introducing nanoinclusions into a thermoelectric material: we noted above that in composites, the propagation and scattering of both phonons and electrons can be affected. Indeed, the nanocomposites with ZrO_2 particles described above [75] showed an increase in the absolute value of thermopower with increasing the particle content. The thermopower changed from -155 to -170 μV K^{-1}, which the authors explained by scattering of charge carriers at inclusion boundaries. As a result of the reduced thermal conductivity and increased thermopower, the thermoelectric figure-of-merit ZT of a composite at 800 K increased from 0.55 in the absence of nanoinclusions to 0.75

for 9% of the ZrO_2 particles. We note that the increase in thermopower due to phonon scattering at heteroboundaries is an important mechanism, and we discuss it in detail below using the example of PbTe-based composites, in which it is most pronounced.

As already noted in Section 2.3, PbTe doped with Ag and Sb forms quaternary compounds $AgPb_{2n}SbTe_{2n+2}$, in which isolated nanometer inclusions of a second phase enriched with Ag and Si lead to an increase in ZT of such a composite to 2.2 at 800 K [19]. The effect of micro- and nanoinclusions on thermoelectric properties has also been observed in other lead telluride-based nanocomposites.

The near doubling of the thermopower was noted in sintered polycrystalline samples of n-PbTe upon decreasing the size of the grains from 4 to 0.7 μm [77], with a concomitant decrease in the electric and thermal conductivity and an increase in the thermoelectric figure-of-merit. The maximum value of the thermoelectric figure-of-merit in fine grain samples turned out to be about 15% higher than in coarse-grain samples with the same charge carrier concentration (of the order of 5×10^{19} cm^{-3}). This positive result was primarily attributed to an increase in the thermopower due to electron scattering on potential barriers near grain boundaries in sintered samples. Such barriers are likely to form by localized states related to point-like defects and grain boundary dislocations [78].

The increase in thermopower in the presence of this scattering mechanism can be qualitatively explained using the 'energy filter' idea [77, 79]. When charge carriers encounter a potential barrier at a grain–grain interface, those of them that have passed over the barrier have a strongly nonequilibrium energy distribution with an increased proportion of high-energy particles, which leads to an increased thermopower [79]. This increase is of a local character, however. When high-energy electrons move to another grain, their nonequilibrium energy distribution gradually relaxes to equilibrium due to scattering on phonons over the length of the electron energy mean free path l_E, and the thermopower resumes its usual value.

Accordingly, a grained material with the grain size $d > l_E$ can be described by mentally dividing it into domains (grains) that have the same thermopower S_g as the material without intergranular barriers has, whereas the thermopower S_b of intergrain regions with a thickness of the order of l_E is increased due to the nonequilibrium electron distribution there. Considering the material as an effective medium, we can estimate the thermopower of the grained material from the expression [77]

$$S = S_g + (S_b - S_g)\,\frac{l_E}{d}\,,$$

where $S_b > S_g$. It follows that the thermopower of a grained material increases with decreasing the grain size d.

The electron energy filtering can be due to causes other than the interaction with barriers. Similar results can be produced by scattering mechanisms that are mainly important for low-energy particles, and relatively less so for high-energy ones. This can easily be understood. For quasielastic scattering mechanisms, the collision rate is proportional to the density of final states and the absolute value squared of the transition matrix element $W(E)$, which for a parabolic dispersion law usually depends on the energy as

$$\left|W(E)\right|^2 \sim E^{-\lambda}\,,$$

where λ is known as the scattering parameter. If the electron scattering is on phonons, then $\lambda = 0$, and if on charged impurities, $\lambda = 2$. For a parabolic electron dispersion law, $g(E) \sim \sqrt{E}$, leading to the well-known expression

$$\tau = \tau_0\, E^{\lambda - 1/2}\,,$$

where the factor τ_0 is energy independent. It is clear from formula (1) for the thermopower of a gas of nondegenerate charge carriers that increasing the scattering parameter leads to an increase in the thermopower.

Experimentally, an increase in the thermopower in comparison with the homogeneous material was observed in nanostructured PbTe samples with grains 30–50 nm in size [78, 80]. The granular size was comparable to the electron mean free path, but greatly exceeded the electron wavelength, preventing the occurrence of quantum dimensional effects; these could only become visible at much smaller inhomogeneity scales, of the order of 10 nm.

To explain this increase, the energy filtering mechanism was invoked. It was established in Ref. [80] that the scattering parameter in a nanogranulated sample increases considerably compared with its value in a homogeneous material with a similar hole concentration ($10^{17} - 10^{19}$ cm^{-3}): in bulk PbTe samples, the scattering parameter is in the range 0.2–0.7, but it increases to 0.7–0.11 in nanogranulated samples. Also, polycrystalline PbTe with Pb inclusions shows an increase in the thermopower in comparison with bulk PbTe samples [81]. Samples with nanometer Pb inclusions and high thermopower have the estimated scattering parameter 3–4, i.e., much larger than for any standard scattering mechanism.

The idea of energy filtering can in principle be implemented, for example, for scattering on a charged impurity. Estimates show, however, that Coulomb scattering in PbTe is significantly suppressed, primarily due to the high dielectric constant (about 400); we also note that the predicted values of Coulomb scattering mobility should be much greater than those observed experimentally.

Direct analysis of scattering on precipitates (modeled by a spherical potential well) using the approach in Ref. [82] to calculate the transport cross section predicts a sufficiently large value, $\lambda = 5/2$, for the scattering parameter; however, the scattering intensity is small under standard conditions, failing to explain the observed value of mobility and thermopower. Other scattering mechanisms (acoustic and optical phonons and neutral impurities) contribute enough to account for the observed mobility values. Besides, for such mechanisms, there is no 'energy filtering' effect that could lead to higher thermopower and power factors. This means that other scattering mechanisms should be considered for materials exhibiting higher power factors.

Results of the measurements of the thermopower, the conductivity, and the Nernst–Ettingshausen coefficient of PbTe films suggest [78] one such unconventional mechanism: asymmetric scattering on potential barriers with the height dependent on the Fermi level position determining the charge of some unknown near-boundary states. A microscopic model for this type of scattering has not yet been developed.

In Ref. [83], spherical metallic inclusions a few nanometers in diameter were taken to act as scatterers in PbTe. Based on the difference in work functions between the semiconductor and the metal, the potential distribution around nanoparticles, the scattering cross section on them, and the corresponding electron mean free path were calcu-

lated numerically. The parameter determined in this way was found to be $\lambda \approx 1.9$. However, the gain in the thermopower due to scattering on metallic nanoparticles was calculated to be insignificant, whereas the conductivity decreased, and therefore the power factor remained virtually unchanged in comparison with PbTe without nanoinclusions.

We note that the thermopower does not always increase as nanoinclusions are introduced. An example is the results of a study [84] of amorphous composites with Ge–Te nanocrystalline inclusions, grown by partially crystallizing the amorphous phase. Transmission electron microscopy revealed that in the amorphous phase, a nanometer-scale phase separation occurs between the glassification and crystallization temperatures, in which nanocrystals 4–8 nm in size form. This does not lead to a higher thermopower but the amorphous nanocrystalline composite annealed for two hours at 443 K has the conductivity and the power factor about three orders of magnitude higher than those in the original amorphous material. Compared with the crystalline alloy GeTe, the amorphous nanocrystalline composite is characterized by the thermal conductivity 0.6 W (m K)$^{-1}$, which is seven times smaller at 300 K, and a thermoelectric figure-of-merit four times higher (but still not large), $ZT = 0.02$. Therefore, the influence of nanoinclusions on the properties of a matrix is not always the same.

Notably, inclusions may also lead to changes unfavorable to the efficiency of thermoelectric conversion. For example, introducing inclusions into the binary compound PbTe decreases the mobility of charge carriers, which negatively affects the thermoelectric figure-of-merit. True, thermoelectric materials in actual use are typically ternary or quaternary alloys of the $Pb_{1-x}Sn_xTe_{1-y}Se_y$ type or other similar group IV–VI compounds with a low crystal thermal conductivity. In alloys, naturally, the mobility is also reduced, and its additional decrease due to nanoinclusions may be expected to be less noticeable than in PbTe.

In concluding the discussion of lead-telluride-based nanocomposites, we note that they also exhibit a decrease in the lattice thermal conductivity characteristic of systems with nanoinclusions. For example, in polycrystalline $Pb_{1.17}Te$ prepared in Ref. [85] by mechanical milling and subsequent plasma sintering, the lattice thermal conductivity proved to be relatively low, 1.11 W (m K)$^{-1}$ at 450; its corresponding increase in the thermoelectric figure-of-merit was to $ZT = 0.64$ at the same temperature. Transmission electron microscopy revealed the presence of randomly distributed nanoinclusions in the material, to which these changes seem to be related.

6.1 Low thermal conductivity materials

The fact that inclusions and other inhomogeneities lead to a significant decrease in the lattice thermal conductivity while virtually not affecting the electronic properties gives rise to the idea of the so-called 'electron crystal–phonon glass' (ECPG) material, in which the electronic properties are those of a crystal, and the phonon ones, those of glass. In such a material, the lattice thermal conductivity decreases substantially without a noticeable decrease in the power factor [24]. Attempts to implement this idea are associated with one of the important new approaches to search for thermoelectric materials, one in which the focus of attention is on discovering or designing materials with low thermal conductivity.

Examples of these include clathrates such as $Sr_4Eu_4Ga_{16}Ge_{30}$ with $\varkappa_L = 0.6$ W (m K)$^{-1}$ [86], filled scutterudites such as $La_{0.75}Th_{0.2}Fe_3CoSb_{12}$ with $\varkappa_L = 1.2$ W (m K)$^{-1}$ [87], and complex bismuth telluride-based materials, for example, $CsBi_4Te_6$ with $\varkappa_L = 0.8$ W (m K)$^{-1}$ [22], the measurement temperature being 300 K in all cases. Among materials suitable for high-temperature operation, we note lanthanum telluride $La_{3-x}Te_4$ with a high concentration of lanthanum vacancies, which are effective phonon scatterers. At the vacancy concentration $x = 0.25$–0.30, the material has the thermal conductivity 0.5–0.9 W (m K)$^{-1}$ in the temperature range 400–1400 K and a high thermoelectric figure-of-merit, $ZT = 1.13$, at 1273 K [88]. The characteristics of a number of other low thermal conductivity materials are presented in Ref. [89].

Besides nanoinclusions, the atoms, molecules, or clusters weakly bound to the rest of the crystal matrix (so-called rattlers) can also act to enhance phonon scattering and to further reduce the lattice thermal conductivity of scutterudites and clathrates. For example, in n-type filled scutterudites $Ba_{0.3}Co_4Sb_{12}$, bivalent Ba easily fills cavities in the structure of the materials and very effectively reduces its thermal conductivity. Introducing a small fraction of Ni into such a scutterudite increases the carrier concentration and the power factor and further reduces the thermal conductivity, leading to a significant increase in the thermoelectric figure-of-merit of the resulting material of the $Ba_{0.3}Ni_xCo_{4-x}Sb_{12}$ type with $0 < x < 0.2$ [90]. Hall measurements showed that adding Ni also increases the role of acoustic phonons compared with charge impurity scattering. The thermoelectric figure-of-merit increases from 0.8 at 800 K for $Ba_{0.3}Co_4Sb_{12}$ to 1.2 in a sample with the Ni content $x = 0.05$.

In [91], molecules of fullerene added to the samples of scutterudite $CoSb_3$ to the content of 6.5 weight % were used as rattlers. The molecules affected both the electronic characteristics and the thermal conductivity of the material. The fullerenes, nearly spherical 60-atom molecules of carbon, formed nanoclusters between the interfaces of $CoSb_3$ grains. It was found that after introducing 5–6% of fullerenes into the material, the dominant scattering mechanism changed from impurity scattering to scattering on grain boundaries. The thermal conductivity decreased with increasing the C_{60} content. Electronic transport at high temperatures was mainly related to the thermal activation via intergrain barriers, and that at low temperatures, to inelastic tunneling. In the fullerene-containing material, it proved possible to achieve a considerable increase in the thermoelectric figure-of-merit compared with pure $CoSb_3$: it was about double for 6.54% C_{60} at 350 K and then decreased monotonically with the temperature to become negligible at about 700 K.

Composites based on the same scutterudite $CoSb_3$ but with ZrO_2 nanoparticles showed a different behavior [92]. The composition formula of the samples was $(CoSb_3)_{1-x}(ZrO_2)_x$ with $x = 0.00$–0.30, and inclusions were 25 nm in size. All the samples studied had their thermopower maximum at 700 K, where the total and electronic thermal conductivities passed a minimum and the thermoelectric figure-of-merit was found to be a maximum. At 700 K, samples prepared free of nanoinclusions had the ZT value equal to 0.18. Compared with this value, the maximum increase in the thermoelectric figure-of-merit (by 11%) occurred at a relatively low inclusion concentration $x = 0.05$. The reason is that at a low content of inclusions, primarily the thermal conductivity decreased, and at a high content, a significant decrease in the electric conductivity occurred, whereas the thermopower depended weakly on the

inclusion concentration. Interestingly, the thermal conductivity of this material varied nonmonotonically with the inclusion content.

Low thermal conductivity is also characteristic of a number of organic compounds, some of which show promise as thermoelectric materials (see Ref. [93]). For example, a fairly high thermoelectric figure-of-merit, $ZT = 0.15$ at room temperature, was observed in copper polyphthalocyanine [94]. The typical parameters of this material are the electric conductivity $\sigma = 0.3$ $(\Omega\ \mathrm{cm})^{-1}$, the thermopower $S = 3100\ \mu\mathrm{V\,K}^{-1}$, and the thermal conductivity $\varkappa = 0.55$ W $(\mathrm{m\ K})^{-1}$. Hence, its thermopower is 15 times higher and thermal conductivity three times lower than in bismuth telluride, but, on the other hand, its electric conductivity is very low. Doping allows increasing the electric conductivity, but causes a large decrease in the thermopower. Unfortunately, organic materials have to date been poorly studied for their thermoelectric properties, nor have methods been sufficiently developed for improving their thermoelectric figure-of-merit.

7. Quantum dot superlattices

Continual improvement in methods for growing semiconductor quantum dot arrays has led to a much deeper understanding of physical processes in quasi-zero-dimensional structures, as well as to an extended range of applications. Until quite recently, most application proposals for quantum dot arrays have been related to optoelectronics [95]. Recent suggestions to use quantum dot arrays for thermoelectric applications changed the situation [34, 96].

On the one hand, quantum dot superlattices are an example of a structure that stops phonons but transmits electrons. Quantum dots randomly distributed in planar layers within a matrix of a different material are effective scatterers of phonons but exert no considerable negative effect on electron transport. On the other hand, quantum dimensional effects determining the properties of carriers in quantum dots can lead to an increase in the power factor and thermoelectric figure-of-merit.

An ordered array of self-organized quantum dots in a molecular-beam epitaxy-grown Bi-doped PbTe-based structure indeed demonstrated remarkable thermoelectric properties [96]. A typical n-type sample of a $PbSe_{0.98}Te_{0.02}$/PbTe superlattice consisted of 8005 periods, each about 13 nm in thickness. Quantum dots formed in a layer with the equivalent composition formula $PbSe_{0.98}Te_{0.02}$. The total thickness of a film was 0.104 nm, and its equivalent composition formula was $PbSe_{0.13}Te_{0.87}$. When used as an n-arm in a thermoelectric refrigerator, these films performed better than standard $(Bi,Sb)_2(Se,Te)_3$. Estimates of ZT for these films ranged between 1.3 and 1.6 at 300 K. Superlattices based on quaternary compounds showed even better performance. Superlattices with PbSnSeTe quantum dots had a thermopower comparable to that of the PbSeTe/PbTe structures described above, but their thermal conductivity was lower and the thermoelectric figure-of-merit was, correspondingly, higher. For such materials of the n-type, the estimated value of ZT reached 2.0 at 300 K, to be compared with $ZT = 0.8$–0.9 obtained for p-type PbSnTe superlattices.

The considerable increase in the thermopower and thermoelectric figure-of-merit of n- and p-type structures compared with PbTe of the same carrier concentration is apparently due to the lattice thermal conductivity decreasing below a value characteristic of homogeneous $PbSe_xTe_{1-x}$ alloys because of the large density of interfaces due to the large number of $PbSe_{0.98}Te_{0.02}$ quantum dots present in PbTe. Also, the presence of an overstoichiometric amount of Te may give rise to a certain additional scattering mechanism for electrons, favorable for increasing the thermopower. We have noted above, however, that the nature of such a mechanism is still unknown.

The mechanism underlying the increase in the thermoelectric figure-of-merit in three-dimensional ordered quantum dot superlattices was studied theoretically in [97]. The calculations were performed for an n-conducting superlattice of Ge and Si quantum dots. Electron energy band calculations showed that if the conditions for the formation of minibands are satisfied, then the electron transport can proceed such that both the carrier mobility and the thermopower increase, and hence so does the thermoelectric figure-of-merit. To achieve the maximum gain, the superlattice parameters should be chosen such that only one miniband, remote from other minibands and of sufficient width (at least a few k_BT), is involved in transport. There is a rather wide range of Fermi level positions for the thermoelectric figure-of-merit of such a superlattice to be one or two orders of magnitude larger than in homogeneous Si. The thermoelectric figure-of-merit shows an especially large increase if it is assumed that the lattice thermal conductivity of the quantum dot lattice decreases compared with its value in homogeneous silicon. Thermal conductivity calculations along the layer stacking direction indeed showed the possibility of a tenfold decrease in $\varkappa_L$ for Ge and Si quantum dot superlattices [34]. In this case, quantum dot superlattices would have a thermoelectric figure-of-merit more than two orders of magnitude higher than in homogeneous silicon.

8. Conclusion

We have reviewed promising approaches to improving the characteristics of thermoelectric materials (primarily, their thermoelectric figure-of-merit) and increasing the efficiency of thermoelectric conversion. Most approaches aim at either increasing the power factor or decreasing the thermal conductivity of a material; or, if possible, at both.

Over the past decades, the study of homogeneous thermoelectric materials of conventional compositions has not led to any significant increase in the power factor. It is therefore understandable that researchers are turning their attention to new, low-thermal-conductivity materials. In recent years, a subject of active discussion has been the idea of using spatially inhomogeneous materials: composites and dimensionally quantized structures based on superlattices, quantum wells, quantum wires, and quantum dots. It was predicted that such structures can exhibit higher power factors and higher thermoelectric figures-of-merit than traditional homogeneous materials. Expectations were only partially met, however; moreover, there are many aspects yet to be clarified regarding how material characteristics, such as chemical composition, doping, and micro- and nano-structure, affect thermoelectric properties.

There is still much work to be done in this area before materials with the high thermoelectric figure-of-merit necessary for wide applications are found or created. Even if this proves impossible, the very importance of the problems warrants the effort.

Acknowledgements. This work was supported by the Federal Target Program "Research and Science Education Personnel of Innovative Russia" for 2009–2013 (contract No. P-2312) and the Russian Foundation for Basic Research (grant No. 09-02-00561).

References

1. Ioffe A F *Poluprovodnikovye Termoelementy* (Semiconductor Thermoelectric Elements) (Moscow: Izd. AN SSSR, 1956)
2. Bell L E *Science* **321** 1457 (2008)
3. Ohita H *Mater. Today* **10** 44 (2007)
4. Tritt T M, Subramanian M A *MRS Bull.* **31** 188 (2006)
5. Ziman J M *Principles of the Theory of Solids* (Cambridge: Univ. Press, 1964) [Translated into Russian (Moscow: Mir, 1966)]
6. Gelbstein Y, Dashevsky Z, Dariel M P *Physica B* **363** 196 (2005)
7. Zvyagin I P *Phys. Status Solidi B* **58** 443 (1973)
8. Mahan G D *J. Appl. Phys.* **65** 1578 (1989)
9. Sofo J O, Mahan G D *Phys. Rev. B* **49** 4565 (1994)
10. Bilc D, Mahanti S D, Kanatzidis M G *Phys. Rev. B* **74** 125202 (2006)
11. Wood C *Rep. Prog. Phys.* **51** 459 (1988)
12. Wrighte D A *Nature* **181** 834 (1958)
13. Akimov B A et al. *Phys. Status Solidi A* **137** 9 (1993)
14. Nemov S A, Ravich Yu I *Usp. Fiz. Nauk* **168** 817 (1998) [*Phys. Usp.* **41** 735 (1998)]
15. Volkov B A, Ryabova L I, Khokhlov D P *Usp. Fiz. Nauk* **172** 875 (2002) [*Phys. Usp.* **45** 819 (2002)]
16. Mott N F, Jones H *The Theory of the Properties of Metals and Alloys* (Oxford: The Clarendon Press, 1936)
17. Heremans J P et al. *Science* **321** 554 (2008)
18. Finch C M, García-Suárez V M, Lambert C J *Phys. Rev. B* **79** 033405 (2009)
19. Hsu K F et al. *Science* **303** 818 (2004)
20. Spitzer D P *J. Phys. Chem. Solids* **31** 19 (1970)
21. Bilc D et al. *Phys. Rev. Lett.* **93** 146403 (2004)
22. Chung D-Y et al. *Science* **287** 1024 (2000)
23. Lykke L, Iversen B B, Madsen G K H *Phys. Rev. B* **73** 195121 (2006)
24. Slack G A, in *Solid State Physics*: *Advances in Research and Applications* Vol. 34 (Eds H Ehrenreich, F Seitz, D Turnbull) (New York: Academic Press, 1979) p. 1
25. Pradel A et al. *Rev. Chim. Miner.* **19** 3 (1982)
26. Wölfing B et al. *Phys. Rev. Lett.* **86** 4350 (2001)
27. Zaitsev V K et al. *Phys. Rev. B* **74** 045207 (2006)
28. Saleh R, Thomas P, Zvyagin I P *Superlattices Microstruct.* **10** 59 (1991)
29. Hicks L D, Dresselhaus M S *Phys. Rev. B* **47** 12727 (1993)
30. Hicks L D, Harman T C, Dresselhaus M S *Appl. Phys. Lett.* **63** 3230 (1993)
31. Hicks L D et al. *Phys. Rev. B* **53** R10493 (1996)
32. Lin Y-M, Sun X, Dresselhaus M S *Phys. Rev. B* **62** 4610 (2000)
33. Lin Y-M, Dresselhaus M S *Phys. Rev. B* **68** 075304 (2003)
34. Khitun A et al. *J. Appl. Phys.* **88** 696 (2000)
35. Harman T C, Spears D L, Manfra M J *J. Electron. Mater.* **25** 1121 (1996)
36. Sofo J O, Mahan G D *Appl. Phys. Lett.* **65** 2690 (1994)
37. Broido D A, Reinecke T L *Phys. Rev. B* **51** 13797 (1995)
38. Broido D A, Reinecke T L *Appl. Phys. Lett.* **67** 100 (1995)
39. Broido D A, Reinecke T L *Appl. Phys. Lett.* **70** 2834 (1997)
40. Broido D A, Reinecke T L *Phys. Rev. B* **64** 045324 (2001)
41. Ridley B K *J. Phys. C* **15** 5899 (1982)
42. Pshenai-Severin D A, Ravich Yu I *Fiz. Tekh. Poluprovodn.* **36** 974 (2002) [*Phys. Semicond.* **36** 908 (2002)]
43. Pshenai-Severin D A, Ravich Yu I *Fiz. Tekh. Poluprovodn.* **38** 1251 (2004) [*Phys. Semicond.* **38** 1212 (2004)]
44. Ivanov Yu V, Vedernikov M V, Ravich Yu A *Pis'ma Zh. Eksp. Teor. Fiz.* **69** 290 (1999) [*JETP Lett.* **69** 317 (1999)]
45. Narayanamurti V et al. *Phys. Rev. Lett.* **43** 2012 (1979)
46. Lee S-M, Cahill D G, Venkatasubramanian R *Appl. Phys. Lett.* **70** 2957 (1997)
47. Touzelbaev M N et al. *J. Appl. Phys.* **90** 763 (2001)
48. Venkatasubramanian R *Phys. Rev. B* **61** 3091 (2000)
49. Landry E S, Hussein M I, McGaughey A J H *Phys. Rev. B* **77** 184302 (2008)
50. Dmitriev A V, Keiper R, Makeev V V *Physica E* **11** 391 (2001)
51. Venkatasubramanian R et al. *Nature* **413** 597 (2001)
52. Venkatasubramanian R et al. *Appl. Phys. Lett.* **75** 1104 (1999)
53. Caylor J C et al. *Appl. Phys. Lett.* **87** 023105 (2005)
54. Bian Z et al. *Phys. Rev. B* **76** 205311 (2007)
55. Sun X, Zhang Z, Dresselhaus M S *Appl. Phys. Lett.* **74** 4005 (1999)
56. Rabin O, Lin Y-M, Dresselhaus M S *Appl. Phys. Lett.* **79** 81 (2001)
57. Mingo N *Appl. Phys. Lett.* **84** 2652 (2004)
58. Mingo N *Appl. Phys. Lett.* **88** 149902 (2006)
59. Walkauskas S G et al. *J. Appl. Phys.* **85** 2579 (1999)
60. Li D et al. *Appl. Phys. Lett.* **83** 2934 (2003)
61. Kittel C *Introduction to Solid State Physics* (New York: Wiley, 1976) [Translated into Russian (Moscow: Nauka, 1978)]
62. Mingo N *Phys. Rev. B* **68** 113308 (2003)
63. Callaway J *Phys. Rev.* **113** 1046 (1959)
64. Mingo N, Broido D A *Phys. Rev. Lett.* **93** 246106 (2004)
65. Broido D A, Mingo N *Phys. Rev. B* **74** 195325 (2006)
66. Mingo N, Broido D A *J. Appl. Phys.* **101** 014322 (2007)
67. Heremans J P et al. *Phys. Rev. Lett.* **88** 216801 (2002)
68. Zhao X B et al. *Appl. Phys. Lett.* **86** 062111 (2005)
69. Hochbaum A I et al. *Nature* **451** 163 (2008)
70. Boukai A I et al. *Nature* **451** 168 (2008)
71. Markussen T, Jauho A-P, Brandbyge M *Phys. Rev. B* **79** 035415 (2009)
72. Cahill D G, Watson S K, Pohl R O *Phys. Rev. B* **46** 6131 (1992)
73. Kim W et al. *Phys. Rev. Lett.* **96** 045901 (2006)
74. Dresselhaus M S et al. *Adv. Mater.* **19** 1 (2007)
75. Chen L D et al. *J. Appl. Phys.* **99** 064305 (2006)
76. Zhu G H et al. *Phys. Rev. Lett.* **102** 196803 (2009)
77. Kishimoto K, Koyanagi T *J. Appl. Phys.* **92** 2544 (2002)
78. Gudkin T S et al. *Fiz. Tekh. Poluprovodn.* **8** 2233 (1974) [*Sov. Phys. Semicond.* **8** 1453 (1974)]
79. Moizhes B Ya, Nemchinsky V, in *Proc. of the 11th Intern. Conf. on Thermoelectrics* (Ed. K R Rao) (Arlington, TX: Univ. of Texas Press, 1992) p. 232
80. Heremans J P, Thrush C M, Morelli D T *Phys. Rev. B* **70** 115334 (2004)
81. Heremans J P, Thrush C M, Morelli D T *J. Appl. Phys.* **98** 063703 (2005)
82. Landau L D, Lifshitz E M *Kvantovaya Mekhanika*: *Nerelyativistskaya Teoriya* (Quantum Mechanics: Non-Relativistic Theory) (Moscow: Nauka, 1974) [Translated into English (Oxford: Pergamon Press, 1977)]
83. Faleev S V, Léonard F *Phys. Rev. B* **77** 214304 (2008)
84. Zhu T J et al. *J. Phys. D* **40** 6094 (2007)
85. Wang H, Li J-F, Kita T *J. Phys. D* **40** 6839 (2007)
86. Cohn J L et al. *Phys. Rev. Lett.* **82** 779 (1999)
87. Sales B C et al. *Phys. Rev. B* **56** 15081 (1997)
88. May A F, Fleurial J-P, Snyder G J *Phys. Rev. B* **78** 125205 (2008)
89. Snyder G J, Toberer E S *Nature Mater.* **7** 105 (2008)
90. Dyck J S et al. *J. Appl. Phys.* **91** 3698 (2002)
91. Shi X et al. *Appl. Phys. Lett.* **84** 2301 (2004)
92. He Z et al. *Nanotechnology* **18** 235602 (2007)
93. Casian A I, in *Thermoelectrics Handbook*: *Macro to Nano* (Ed. D M Rowe) (Boca Raton: CRC/Taylor and Francis, 2006) Ch. 36
94. Zabrowska M *High Temp. High Press.* **7** 215 (1985)
95. Huffaker D L et al. *Appl. Phys. Lett.* **73** 2564 (1998)
96. Harman T C et al. *Science* **297** 2229 (2002)
97. Balandin A A, Lazarenkova O L *Appl. Phys. Lett.* **82** 415 (2003)